Intrinsic defects of $TiO_2(110)$: Interaction with chemisorbed O_2, H_2, CO, and CO_2

W. Göpel and G. Rocker
Physics Department, Montana State University, Bozeman, Montana 59717

R. Feierabend
Institute of Physical Chemistry, University of Hannover, D-3000 Hannover, West Germany
(Received 18 March 1983)

The interaction of $TiO_2(110)$ with O_2, H_2, CO, and CO_2 was studied by means of low-energy electron diffraction, x-ray photoelectron spectroscopy, electron energy-loss spectroscopy, thermal desorption, electron paramagnetic resonance, and measurements of changes in surface conductivities, $\Delta\sigma$, and work functions, $\Delta\varphi$, for $300 \leq T \leq 1000$ K with particular emphasis on surface reactions involving intrinsic surface defects $2Ti^{3+} \cdot V_O^{(+)}$. The defects are thermodynamically stable at high temperatures and act as donors and specific adsorption sites for H_2 and CO. Surface and subsurface reactions involving O_2, H_2, CO, and CO_2 can be separated from each other by analyzing the $\Delta\sigma$ and $\Delta\varphi$ effects in a charge-transfer model, which takes into account surface and bulk electronic states in the band gap attributed to the different defects formed during the interaction.

I. INTRODUCTION

Studies of electronic charge transfer during adsorption of H_2, O_2, CO, and CO_2 at TiO_2 surfaces are of principal interest for an atomistic understanding of practically important TiO_2 applications, e.g., in heterogeneous catalysis, photochemical decomposition of water, the design of specific gas sensors, etc.[1] From the basic science point of view, studies at (110) single-crystal TiO_2 surfaces are of particular interest. First, this surface is the thermodynamically most stable surface of TiO_2 (Refs. 2–4) and is expected to make possible the study of reversible solid-gas interactions. Second, ideal $TiO_2(110)$ surfaces show no intrinsic surface states in the band gap.[3–5] States may, however, be induced by the formation of either intrinsic point defects of the ideal TiO_2 lattice, such as vacancies or interstitial atoms, or of extrinsic defects associated with foreign atoms.[4–10] Third, we expect our earlier charge-transfer model[11,12] to adequately describe chemisorption effects in the electronic structure of ideal, i.e., defect-free $TiO_2(110)$ in terms of "localized" variations in the electronic charge redistribution in the valence-band range and of "delocalized" changes in the concentration of conduction-band electrons, the latter resulting from donor and acceptor states of extrinsic point defects in the band gap. Experimentally observed deviations from results expected on the basis of this charge-transfer model can, therefore, be attributed to changes in the concentration of intrinsic point defects.[13]

Intrinsic point defects can easily be created in TiO_2. Their concentration determines charge-transfer effects during chemisorption, e.g., due to their influence on the bulk Fermi-level position. Point defects at the surface in particular may act as specific adsorption sites for certain molecules.[4,9,10] TiO_2 is known to have high diffusion coefficients for point defects in the bulk[8,14–20] and even to decompose at high temperatures and low oxygen pressures or at elevated temperatures in the presence of reducing gases,[4,8,9–11,17–25] thereby forming suboxides TiO_x with $x < 2$.[17,26,27] We, therefore, expect reactions between surface complexes and bulk defects in subsurface regions to occur even at temperatures as low as 300 K. We also expect a control of concentrations of intrinsic defects at the surface to be possible by high-temperature pretreatment under thermodynamically controlled conditions and subsequent quenching.

In this paper we present studies on the interaction of $TiO_2(110)$ with O_2, H_2, CO, and CO_2 that were performed with different concentrations of intrinsic defects at the surface. We will develop a concept to separate chemisorption steps from chemical reactions involving intrinsic defects at or near the semiconductor surface. For interactions with O_2, H_2, and CO in particular, intrinsic surface defects will be shown to act as "active sites" for chemisorption and/or decomposition of the molecules.

The concept to be developed in this study can be applied to any semiconductor chemisorption system if the concentration of intrinsic electronic states is negligible in the band gap of ideal surfaces. This is generally the case for compound semiconductors with high ionicity in the absence of intrinsic point defects. Binary metal oxides in particular represent the most important class of semiconductors of this kind, and amongst them $TiO_2(110)$ will be shown to serve as an ideal "prototype surface" to study gas-solid interactions involving surface defects.

II. EXPERIMENTAL

Most of the studies were done in a modified Varian 120 low-energy electron diffraction–Auger-electron spectroscopy (LEED–AES) system at a base pressure less than 10^{-10} mbar. Thermal desorption spectroscopy (TDS), LEED, AES, and measurements of changes in surface potentials, $\Delta\varphi$, and conductivities, $\Delta\sigma$ (the latter with the four-point van der Pauw method[28]), during chemisorption of particles were carried out at $TiO_2(110)$ single-crystal

surfaces with an experimental setup as described in detail earlier.[29] X-ray photoelectron spectroscopy (XPS) and electron energy-loss spectroscopy (EELS) were done in a separate chamber. In a UHV molecular-flow apparatus, TDS experiments could be performed with high accuracy ($\Theta_{min}=10^{-4}$ monolayer).[30] Another independent UHV setup made possible the determination of paramagnetic defects and/or chemisorption complexes by means of electron paramagnetic resonance (EPR).[31]

III. RESULTS

A. Sample preparation and intrinsic defects

The TiO_2 crystals were cut to wafers $10\times10\times0.8$ mm^3 in size, polished, high-temperature and oxygen treated to remove the main carbon contaminations [$P(O_2)=5\times10^{-4}$ Pa, $T=600$ K, $t=2$ h], subsequently argon bombarded under UHV conditions (6×10^{-5} Pa, 500 V, 0.3 μA, 600 K, 20 min), and then exposed to oxygen (4×10^{-3} Pa, 2 h, 600 K) to anneal the nonstoichiometry, i.e., the oxygen deficiency due to defects near the surface which result from Ar^+-ion bombardment.[4] Defects could also be produced by an entropy-driven preferred desorption of molecular oxygen under UHV at high temperatures ($T>900$ K). As we will see in the following, this thermal treatment leads to one type of well-defined defect.

We identified intrinsic defects with different techniques. In EPR, thermally produced defects give rise to a symmetric signal with a g value close to the free-electron value and negligible difference in the g value between surface and bulk defects as checked by the time dependence of EPR spectra during subsequent annealing of the defects in O_2 at 300 K. As will be shown in more detail below, these defects are most probably oxygen vacancies with one free-electron-like charge trapped in their first ionization stage.

In line with earlier studies,[4,9] we observed even more pronounced changes in the stoichiometry and significantly higher defect concentrations after ion bombardment. In XPS high concentrations of surface defects lead to pronounced shifts in the Ti $2p$ core levels to lower binding energies (curve b in Fig. 1) if compared with the defect-free surface (curve a in Fig. 1). In addition, defects lead to a separate peak in the Auger $L_3M_{23}V$ transition with a kinetic energy 420.1 eV above the main peak at 414.8 eV, which is attributed to transitions at defect-free surfaces. The EELS results indicate electronic states to occur in the band gap 0.3 eV below the conduction band in the presence of surface defects. These states can be shown to determine the energy of the separate AES peak mentioned above.[32]

In subsequent oxygen-exposure experiments, rapid reactions restore the stoichiometry at the surface and anneal defect-related structures in EELS, AES, and XPS, as well as in EPR, as mentioned above. As an example, curve c in Fig. 1 shows XPS results with a reduced surface-related Ti $2p_{3/2}$ feature at 458 eV if compared with curve b. In this experiment, oxygen was added at low temperatures ($T=150$ K, $P=2\times10^{-4}$ Pa) and the XPS change was observed immediately thereafter. This annealing process is expected to basically involve surface defects only. After longer exposure times at elevated temperatures ($t>20$ min, $T=600$ K), subsurface defects are also annealed, and the original EELS or XPS spectra (curve a) of the ideal surface are obtained again. Details on these electron spectroscopic studies will be published elsewhere.[32]

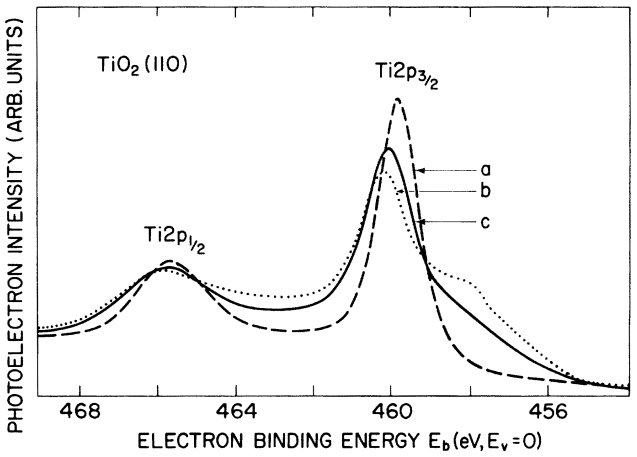

FIG. 1. XPS electron binding energies for Ti $2p_{1/2}$ and Ti $2p_{3/2}$ at different concentrations of intrinsic defects. Curve a represents the stoichiometric surface, curve b is the surface with a high defect concentration obtained by Ar^+-ion bombardment. Thermally produced defects after high-temperature annealing in UHV lead to an increase of the feature near 458 eV only. Curve c is the partially annealed surface. Further details are explained in the text.

An analysis of our LEED experiments leads to an estimate of concentrations of irregularly bound surface atoms after various sample pretreatments. This concentration is 1 to 2 orders of magnitudes higher after Ar^+-ion bombardment (for experimental conditions as mentioned above) if compared with the situation after high-temperature UHV pretreatment to produce surface defects at $T\leq1310$ K. Comparative studies of the spatial distribution of LEED reflexes at different LEED voltages, of the energy range of XPS core-level shifts, of the spectrum of g values in EPR, and of $\Delta\sigma$ and $\Delta\varphi$ effects during low-temperature exposure of O_2 to defect surfaces (cf. Sec. III B), gave clear evidence that a variety of different types of defects is produced by Ar^+ bombardment, whereas high-temperature—low-oxygen pressure pretreatment leads to reproducible surface structures which can be explained by the occurrence of one type of defect, i.e., oxygen vacancies.

In contrast to earlier TiO_2 studies, in which defects were produced by Ar^+-ion bombardment,[4,9] we are now able to produce well-characterized defect structures of TiO_2(110) in a thermodynamically controlled way. The following results and discussion will deal exclusively with such prepared TiO_2 surfaces.

B. Oxygen-exposure experiments

The most sensitive experimental tools to detect small concentrations of intrinsic defects are measurements of

conductivity ($\Delta\sigma$) and surface potential ($\Delta\varphi$) changes during the interaction of oxygen with defect surfaces. These $\Delta\sigma$ and $\Delta\varphi$ changes are pronounced since the defects are *F*-center-like surface donors (cf. Sec. IV B 1) that can be annealed by oxygen.

Characteristic results on the pressure dependence at constant temperatures (303 K) and on the temperature dependence at constant pressures (6.7×10^{-5} and 6.7×10^{-4} Pa) are given in Figs. 2 and 3, respectively, for TiO_2 samples prepared at 600 K in 4×10^{-3} Pa O_2 for 2 h. In contrast to the surface potential, the conductivity drifted even under the best vacuum conditions, as indicated in curve 0 of Fig. 2. This drift is determined by the O_2 partial pressure in the residual gas and cannot be influenced by CO, H_2, or CO_2 partial pressures up to 10^{-7} Pa. At temperatures above 373 K, $\Delta\varphi$ changes are insignificant, whereas the corresponding $\Delta\sigma$ changes become pronounced (cf. Fig. 3). For higher concentrations of intrinsic defects, prepared by sample pretreatments at higher temperatures and/or lower O_2 partial pressure, corresponding $\Delta\sigma$ and $\Delta\varphi$ changes are larger. An analysis of the different temperature dependences of $\Delta\sigma$ and $\Delta\varphi$ in Sec. IV B will make possible the separation of chemisorption steps from surface and bulk reaction steps involving annealing of intrinsic defects during oxygen exposure.

C. Interaction with H_2, CO, and CO_2

Chemisorption of those particles forming donor- or acceptor-type surface complexes is also expected to lead to

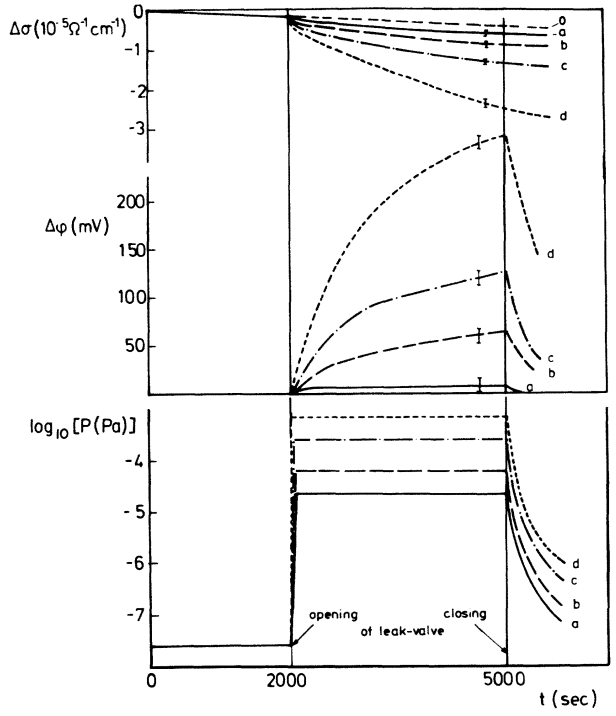

FIG. 2. Changes in the conductivity $\Delta\sigma$ and surface potential $\Delta\varphi$ during exposure of TiO_2(110) to molecular oxygen at different pressures P with *a*, $P=6.7\times10^{-6}$ Pa; *b*, $P=1.2\times10^{-5}$ Pa; *c*, $P=6.7\times10^{-5}$ Pa; *d*, $P=6.7\times10^{-4}$ Pa. Measurements were done at 303 K.

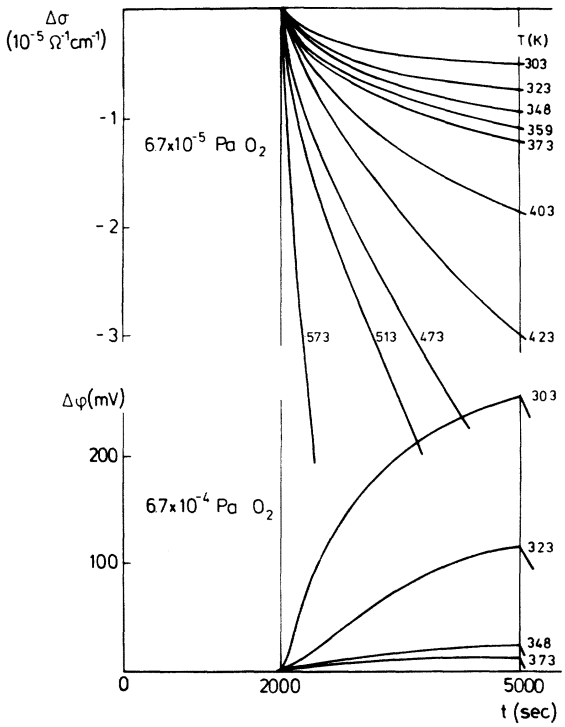

FIG. 3. Changes in conductivity $\Delta\sigma$ and surface potential $\Delta\varphi$ during oxygen exposure at different temperatures.

$\Delta\sigma$ and $\Delta\varphi$ effects due to charge transfer involving conduction electrons. These effects are expected to depend on the concentration of the above-mentioned charged intrinsic surface defects. We have, therefore, studied the interaction of different gases for different concentrations of intrinsic surface defects at TiO_2(110).

Figure 4 shows characteristic $\Delta\sigma$ and $\Delta\varphi$ results for the interaction of TiO_2(110) surfaces with H_2, CO, and CO_2 at various pressures and temperatures. The CO_2 shows neither $\Delta\varphi$ nor $\Delta\sigma$ effects at pressures up to 10^{-3} Pa and temperatures between 300 and 500 K. The $\Delta\varphi$ effects of CO are also negligible in this temperature range, whereas corresponding $\Delta\sigma$ effects can be measured as shown by the dash-dotted lines in the upper part of Fig. 4. The $\Delta\varphi$ effects during H_2 interaction are independent of the temperature between 303 and 348 K and become negligible above about 370 K.

Subsequent TDS experiments make possible the determination of coverages of adsorbed species. The TDS results, after different exposure times t during adsorption, indicate adsorption equilibria to be established for all gases except O_2 after $t\geq500$ sec. Figures 5–7 show the coverage Θ of H_2, CO, and CO_2 adsorption species as a function of pressure at constant temperature, i.e., adsorption isotherms, as determined from the integrated pressure increase during TDS experiments in the molecular flow apparatus after 3×10^3 sec exposure time. In TDS only the previously adsorbed molecules H_2, CO, and CO_2, and no reaction products, such as H_2O (after H_2 exposure) or CO_2 (after CO exposure), were observed. During CO exposure, however, small amounts of CO_2 were observed in the mass spectrometer (less than 10 ppm of the CO pres-

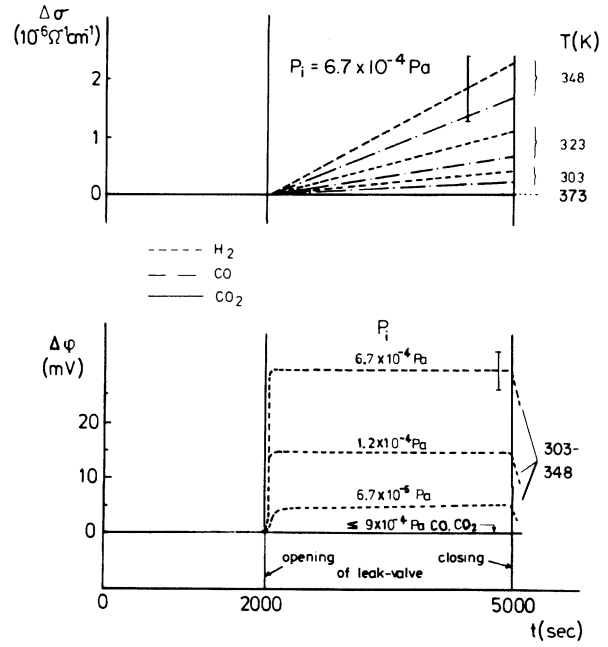

FIG. 4. Changes in conductivity $\Delta\sigma$ and surface potential $\Delta\varphi$ during interaction of $TiO_2(110)$ with H_2, CO, and CO_2. Further explanations are given in the text.

sures), which decayed with relaxation times in the order of 50 sec.

The value $\Theta=1$ in Figs. 5–7 corresponds to $n_s^{ad}=1.48\times10^{15}$ particles per cm^2. This corresponds to one adsorption complex per titanium surface atom. From adsorption isotherms and

$$q_{st}=-R\left[\frac{d\ln P}{d(1/T)}\right]_\Theta, \tag{1}$$

we determined isosteric heats of adsorption $q_{st}(H_2)=83.3$, $q_{st}(CO)=79.8$, and $q_{st}(CO_2)=63.3$ kJ mol^{-1}.

The CO_2 adsorption isotherms are independent of the surface nonstoichiometry, i.e., the concentration of oxygen vacancies prepared by high-temperature pretreatment, whereas the H_2 as well as CO adsorption isotherms depend on the high-temperature pretreatment. The results in

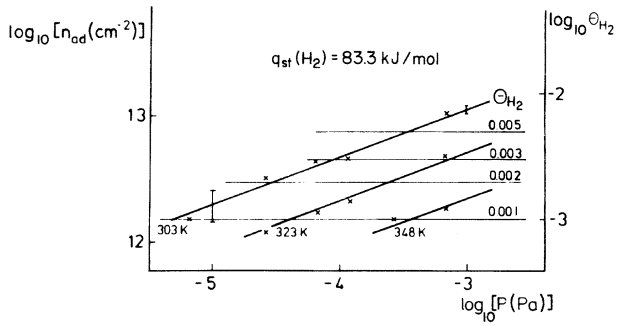

FIG. 5. Adsorptions isotherms for H_2 interaction with $TiO_2(110)$.

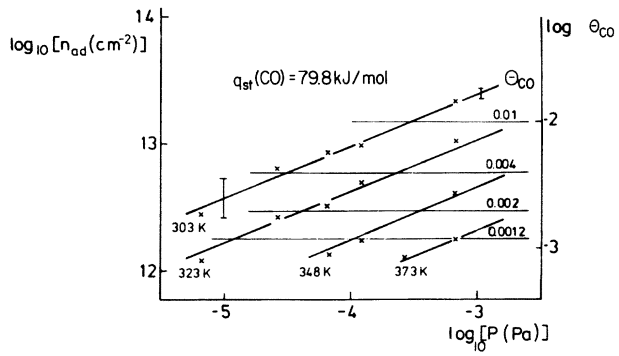

FIG. 6. Adsorption isotherms for CO interaction with $TiO_2(110)$.

Figs. 5 and 6 are obtained after high-temperature pretreatment at 600 K, $P(O_2)=5\times10^{-4}$ Pa, and $t=2$ h. Higher (or lower) temperatures as well as lower (or higher) oxygen pressures at constant temperature lead to an increase (or decrease) of corresponding equilibrium concentrations of adsorbed H_2 and CO in subsequent low-temperature ($T<373$ K) adsorption experiments. In all cases, the TDS experiments after low-temperature gas exposure did, however, indicate constant coverages Θ ("equilibria," although $\Delta\sigma$ and/or $\Delta\varphi$ may not be constant) to be obtained after 500 sec with Θ given by the high-temperature pretreatment as well as by pressure and temperature during subsequent low-temperature exposure. For maximum TDS temperatures below 575 K, coverages of H_2, CO, and CO_2 could be reproduced in subsequent adsorption experiments. Activation energies $\tilde{E}^{des}$ of thermal desorption are listed in Table I.

IV. DISCUSSION

A. Chemisorption and the charge-transfer model

We will tentatively evaluate the results on changes in surface conductivities $\Delta\sigma$ and surface potentials $\Delta\varphi$ for a given coverage Θ of adsorbed particles by assuming a simple charge-transfer model to be applicable to describe

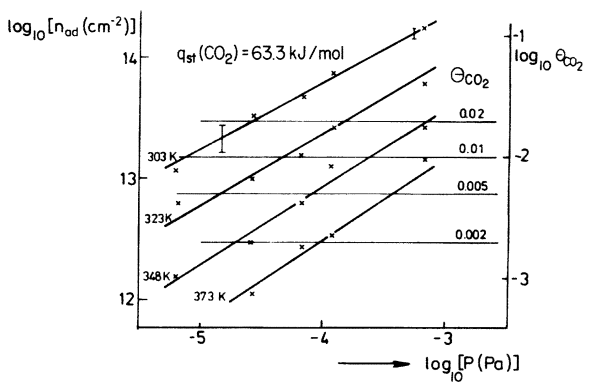

FIG. 7. Adsorption isotherms for CO_2 interaction with $TiO_2(110)$.

TABLE I. Partial charge δ, dipole moments μ^{ad}, isosteric heats of adsorption q_{st}, activation energies of desorption $\tilde{E}^{des}$, and initial sticking coefficients S_0, attributed to the interaction of different particles with TiO_2(110). For comparison, results from our earlier studies on ZnO(10$\bar{1}$0) are also given. Values at 300 K, $P=6.7\times10^{-4}$ Pa, $t=3\times10^3$ sec exposure time.

	δ		μ^{ad}/ϵ_s (Debye)		q_{st} (kJ mole^{-1})		$\tilde{E}^{des}$ (kJ mole^{-1})		S_0	
	TiO_2 (110)	ZnO (10$\bar{1}$0)	TiO_2 (110)	ZnO (10$\bar{1}$0)	TiO_2 (110)	ZnO (10$\bar{1}$0)	TiO_2 (110)	ZnO (10$\bar{1}$0)	TiO_2 (110)	ZnO (10$\bar{1}$0)
O_2	-1	-1	0	0			94	106	8×10^{-5}	2×10^{-6}
H_2	$+1\times10^{-2}$	$+1$	12	-1.8	83		102	96	1×10^{-6}	0.3(H)
CO_2	0	-4×10^{-3}	0	10	63	70	96	87	1×10^{-2}	0.6
CO	$+6\times10^{-3}$		5		80		98		2×10^{-5}	

changes in the electronic structure of TiO_2(110) during chemisorption.[11,12] In this model changes in concentrations of free electrons upon chemisorption are formally described by the formation of donor- or acceptor-type extrinsic defects. These defects introduce electronic states in the empty gap of ideal TiO_2(110). They may be characterized by an energy E_{ss}^{eff} and an ionization probability given by Fermi statistics. The key parameters characterizing the chemisorption complexes are the partial charge δ and the dipole moment μ^{ad}.

1. *Partial charges* δ

According to the relations

$$\delta = Q_{ss}/en_s^{ad} \tag{2}$$

and

$$f(E_{ss}^{eff}-E_F)=\left[1+\exp\left[\frac{E_{ss}^{eff}-E_F}{kT}\right]\right]^{-1}=\begin{cases}-\delta\\1-\delta\end{cases} \tag{3}$$

for acceptors and donors, respectively, the occupation probability $f(E_{ss}^{eff}-E_F)$ determines the partial charge δ formally attributed to defect formation. Here e is the elementary charge, E_F is the Fermi level, and Q_{ss} is the surface charge per unit area, which is trapped during the chemisorption of n_s^{ad} particles per unit area. The general expression for Q_{ss} is

$$Q_{ss}=e\left[\int_{-\infty}^{\infty} D_D(E)f(E_F-E)dE - \int_{-\infty}^{\infty} D_A(E)f(E-E_F)dE\right], \tag{4}$$

with $D_D(E)$ and $D_A(E)$, respectively, the donor and acceptor densities of surface states per unit area.

We will now determine δ from experimental $\Delta\sigma$ and Θ results. In a first step, we determine the changes ΔN in the effective density of free electrons per unit area in the space-charge layer from experimentally determined $\Delta\sigma$ results. We introduce the excess surface conductivity[11]

$$\Delta\sigma_s=\Delta\sigma\, d=e\mu_e\,\Delta N+e\mu_p\,\Delta P\ . \tag{5}$$

The value $\Delta\sigma_s$, in contrast to $\Delta\sigma$, is independent of the sample geometry. In Eq. (5), μ_e and μ_p denote mobilities of electrons and defect electrons, respectively, ΔP is the analog of ΔN for defect electrons, and d is the sample thickness. The further evaluation is simplified significantly by the experimental fact that ΔP is negligible for all preparation conditions of our samples.

A large amount of work has been done[33] to study conductivities and mobilities in TiO_2 for various bulk defect concentrations. In our evaluations, values for the mobility $\mu_e(T)$ are taken from the literature by assuming that bulk mobilities are not changed near the surface. For comparable sample preparation and the temperature range between 300 and 600 K relevant for our studies, $\mu_e=1.0\times10^6\,(T/K)^{-2.5}\ cm^2\,(V\,sec)^{-1}$ holds.[34]

In the next step, we determine energy positions and concentrations of bulk donors (acceptors can be neglected) from the experimental temperature dependence of bulk conductivities and mobilities of our samples. The following equilibrium conditions hold for donor-type bulk defects:

$$V_O^{\,0}\rightleftarrows V_O^{\,+}+e\ , \tag{6a}$$

$$V_O^{\,+}\rightleftarrows V_O^{\,2+}+e\ , \tag{6b}$$

where $V_O^{\,0}$ is the doubly occupied, $V_O^{\,+}$ is the singly ionized, and $V_O^{\,2+}$ is the doubly ionized oxygen vacancy. If the energy difference between the lower conduction-band edge and the Fermi level is large as compared to the thermal energy kT, the bulk concentration of free conduction electrons, n_b, is approximately given by

$$n_b=N_c\exp[(E_F-E_c)/kT]\ , \tag{7a}$$

with

$$N_c=2(2\pi m_{eff}kT/h^2)^{3/2}\ . \tag{7b}$$

Here $m_{eff}=20m_e$ (Ref. 35) is the effective mass of conduction-band electrons and E_C the conduction-band edge.

The equilibrium constants K_{D1} and K_{D2} attributed to Eqs. (6a) and (6b) are as follows:

$$K_{D1}=\frac{N_{D1}n_b}{N_D^0}=2N_c\exp\left[\frac{E_{D1}-E_C}{kT}\right], \tag{8a}$$

$$K_{D2}=\frac{N_{D2}n_b}{N_{D1}}=\tfrac{1}{2}N_c\exp\left[\frac{E_{D2}-E_C}{kT}\right], \tag{8b}$$

where N_D^0 is the density of doubly occupied, N_{D1} of singly ionized, and N_{D2} of doubly ionized donors, and $E_{D1,2}-E_C$ is the first (second) ionization potential of the donor-type oxygen vacancy relative to the conduction-band edge with

$$N_D=N_D^0+N_{D1}+N_{D2}\ , \tag{9}$$

as well as the charge neutrality condition

$$n_b=2N_{D2}+N_{D1}\ . \tag{10}$$

By assuming that no acceptors are involved we find

$$n_b=N_D K_{D1}\frac{2K_{D2}+n_b}{n_b^2+n_b K_{D1}+K_{D1}K_{D2}}\ . \tag{11}$$

With n_b from experimental conductivity and mobility data, Eq. (11) can be solved numerically by fitting the unknown parameters E_{D1}, E_{D2}, and N_D to the temperature dependence of n_b.

In the third step, changes in space-charge densities Q_{sc} per unit area are calculated as a function of excess surface conductivity $\Delta\sigma_s$. Each value $\Delta\sigma_s$ (and hence Q_{sc}) corresponds to a certain band bending V_s induced by chemisorption. We normalize $V_s(\Theta=0)=0$ in the absence of absorbed species. In the calculation we solve the Poisson equation by taking into account the spatial variation of effective ionization of bulk donor and acceptor states near the surface for each value V_s as follows: For our semiconductor with donor-type flaws having two ionization stages, the change in the space-charge density due to band bending is given by

$$q_{sc}=-e[n(z)-N_{D1}(z)-2N_{D2}(z) -(n_b-N_{D1}-2N_{D2})]\ , \tag{12}$$

where z is the coordinate perpendicular to the surface with $z=0$ at the surface, and $\lim_{z\to\infty}n(z)=n_b$ and $\lim_{z\to\infty}N_{D1,2}(z)=N_{D1,2}$ (both values being constant deep in the bulk). Any variation of the electrostatic potential parallel to the surface is neglected.

The band bending $V(z)$ with $V_s=V(z=0)$ is related to q_{sc} via the Poisson equation

$$\frac{d^2V(z)}{dz^2}=\frac{-q_{sc}}{\epsilon\epsilon_0}\ . \tag{13}$$

Introducing $v=eV/kT$, assuming

$$n(V)=N_c f(E_c-eV-E_F)\ ,$$

and forming analog expressions for $N_{D1,2}(V)$, we can solve Eq. (13) for dV/dz analytically and, hence, find the space-charge density Q_{sc} per unit area by integrating

$$Q_{sc}=\int_0^\infty q_{sc}(z)dz=\frac{\epsilon\epsilon_0 kT}{e}\left[\frac{dv}{dz}\right]_{z=0}\ . \tag{14}$$

The excess surface conductivity $\Delta\sigma_s$ can be expressed by

$$\Delta\sigma_s=\mu_e e\int_{v_s}^0\frac{n(v)-n_b}{dv/dz}dv\ . \tag{15}$$

This equation can be evaluated numerically.

Quantitative results will now be given. Figure 8 shows

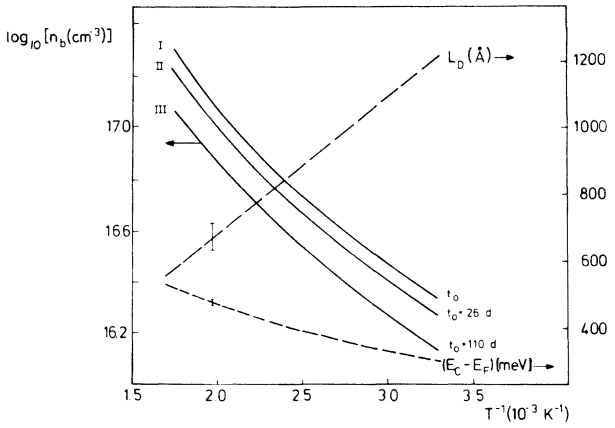

FIG. 8. Concentration n_b of free electrons, Debye length L_D, and position of the Fermi level with respect to the conduction-band edge E_C-E_F as a function of temperature.

the bulk concentration of free electrons n_b for different samples as a function of temperature as determined from conductivities and mobilities for $V_s=0$. From $n_b=f(T)$, we determine the position of the Fermi level E_F relative to the conduction band E_C from Eq. (7). We calculate the Debye length L_D as a characteristic screening length for trapped surface charges from

$$L_D=[2\epsilon\epsilon_0 kT/(e^2n_b)]^{1/2}\ . \tag{16}$$

Results for (E_C-E_F) and L_D calculated for sample I at various temperatures are also shown in Fig. 8. Following the evaluation scheme as described above, the bulk conductivity data are described by donor-type flaws with two ionization energies, $E_{D1}-E_C=-325$ meV and $E_{D2}-E_C=-515$ meV, and with concentrations between 3.8×10^{16} cm^{-3} (sample I) and 2.44×10^{16} cm^{-3} (sample III). As will be discussed in the next section, these donors are most probably oxygen vacancies $V_O{}^0$ and $V_O{}^+$, respectively, associated with titanium. Donor concentrations gradually decrease during annealing of the defects in low-temperature ($T=300$ K) reactions with oxygen from the residual gas. This shifts curve I in Fig. 8 after long measuring times to lower values of n_b with examples represented by curves II and III. At elevated temperatures and high O_2 partial pressures, curve I can be shifted down in significantly shorter times. At temperatures above $T=900$ K and $P(O_2)<10^{-7}$ Pa, curve I is shifted up as the result of formation of additional bulk defects, the thermodynamically stable concentration of which increases with T and decreases with $P(O_2)$.

Charge neutrality requires $Q_{sc}=-Q_{ss}$ with Q_{ss} as the surface concentration of trapped charges. By using Eqs. (2) and (3), the values for partial charges δ and surface state energies E_{ss}^{eff} in Table I have been determined from Q_{ss} and n_s^{ad} (or Θ). Here n_s^{ad} was taken from TDS results in Figs. 5–7.

2. *Dipole moments* μ^{ad}

Dipole moments attributed to the adsorption complexes are introduced to explain formally the discrepancy be-

tween the theoretically expected band bending V_s and the experimentally determined changes in the work function

$$\Delta\phi = e\,\Delta\varphi = -eV_s + \Delta\chi \ . \tag{17}$$

We assume in the low-coverage range with negligible dipole-dipole interaction

$$\mu^{ad} = \epsilon_s \epsilon_0 \Delta\chi / n_s^{ad} \ , \tag{18}$$

where ϵ_s is the dielectric constant at the surface. In this approach μ^{ad} describes changes in the electron affinity $\Delta\chi$ at the surface during adsorbate formation.

Results for μ^{ad} are also shown in Table I together with q_{st} results, activation energies of desorption $\tilde{E}_{des}$ as determined from TDS and initial sticking coefficients S_0. The latter determine rates of adsorption in the zero-coverage limit[13,36] and were calculated from $d(\Delta\sigma_s)/dt$ for $\Theta \rightarrow 0$ by using Eq. (2) and assuming that the above calculated δ values attributed to the chemisorption complex can be extrapolated to zero coverage, i.e., $V_s = 0$. The results for H_2 and CO adsorption correspond to measurements at TiO_2 samples after high-temperature pretreatment as in Figs. 5 and 6.

3. *Electronic states of intrinsic and extrinsic defects*

Figure 9 shows a survey on the different bulk and surface electronic states determined so far to formally describe bulk conductivities and conductivity changes as well as surface potential changes during the exposure of TiO_2(110) to different gases. High-temperature pretreatment of the sample leads to thermodynamically stable donor concentrations in the bulk with ionization energies E_{D1} and E_{D2}. During cooling to low temperatures these defects are quenched and lead to kinetically controlled annealing processes in the presence of oxygen. As shown in more detail in Fig. 8, the bulk Fermi level E_F is temperature dependent. As a result, even the upper bulk-donor level is not completely ionized at 300 K, as can be deduced from the value of $f(E)$ of the Fermi function in the right part of Fig. 9. The paramagnetic species observed in EPR, therefore, represent the fraction $f(E)$ of the total defect concentration only. The band gap is free from intrinsic surface states attributed to the ideal surface. The band bending, which depends on the coverage of certain adsorbed species, is not shown in this schematic figure.

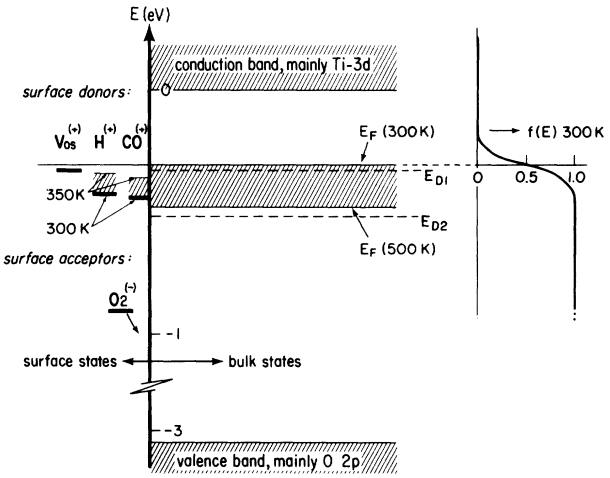

FIG. 9. Schematic energy diagram characterizing surface and bulk electronic states of TiO_2(110). Surface-state positions ($E_{ss}^{eff} - E_F$) at 300 K are as follows: 700 meV ($O_2^{(-)}$) (Ref. 2), −115 meV ($H^{(+)}$), −133 meV ($CO^{(+)}$), −25 meV ($V_{Os}^{(+)}$), for corresponding band bending eV_s (after 3×10^3 sec exposure time at $P = 6.7\times10^{-4}$ Pa) of −270 meV ($O_2^{(-)}$), +31 meV ($H^{(+)}$), +11 meV ($CO^{(+)}$). For further explanations, see text.

Acceptor states formally attributed to $O_2^{(-)}$ are introduced by chemisorption of O_2. Donor states are formally attributed to $H^{(+)}$ and $CO^{(+)}$ surface complexes. These acceptors and donors are extrinsic defects in contrast to the intrinsic defect $V_{Os}^{(+)}$. The oxygen vacancies $V_{Os}^{(+)}$ at the surface are introduced by high-temperature pretreatment and will be discussed in more detail below. Even under flat-band condition, the different surface donors are partially ionized only at 300 K. With increasing donor concentration and hence decreasing surface potential, the partial charge δ decreases.

In the context of charge transfers involving conduction electrons, $V_{Os}^{(+)}$ may be formally described as a "negatively" absorbed species. The thermodynamic concept of treating negatively absorbed species has been introduced in our earlier study on ZnO surface defects.[13] It can also be applied to defects on TiO_2(110).

B. Intrinsic defects as "active sites" for chemisorption

Surface donor levels attributed to chemisorption of H_2 and CO, as determined in the last chapter, characterize adsorption at intrinsic defect sites of the surface. As pointed out in Sec. III C, these two gases do not interact with the surface in the absence of defect sites. Consequently, trapping of conduction electrons in corresponding $H^{(+)}$ or $CO^{(+)}$ chemisorption levels is not observed under these conditions.

1. *The structure of surface-intrinsic defects*

We will now discuss the physical origin of intrinsic surface defects on TiO_2(110). Our experiments indicate paramagnetic defects (from EPR) of donor type (from $\Delta\sigma$) with lowered Ti $2p_{3/2}$ binding energies in their vicinity (from XPS) that lead to an increase in reactivity of the ideal surface (from $\Delta\sigma$ and $\Delta\varphi$ during O_2, H_2, and CO exposure). Electronic states in the gap have been associated with the existence of intrinsic defects.[4,32] Our EELS studies indicate defect-related gap states 300 meV below the conduction band. From earlier studies on the defect formation at TiO_2(110),[6] it is fairly well established that filled band-gap defect surface states correspond to $Ti^{3+}\cdot V_{Os}$ vacancy complexes, although the detailed geometry of those complexes is not precisely known. The most probable type of surface defect at TiO_2(110) is shown later in Fig. 11 by the missing O ion that bridges two sixfold-coordinated Ti ions. When a bridging O ion is removed, the two neighboring Ti ions become fivefold coordinated. However, observations on nearly perfect TiO_2 (110) and (100) surfaces

show that fivefold coordination may not be sufficient to completely populate band-gap surface states in n-type material. This explains why the donor level in Fig. 9 as the first ionization level is partly filled only. For this defect the two Ti ions are very poorly screened from each other, which is somewhat analogous to the situation in bulk Ti_2O_3. The poorly screened pair of Ti ions at the defect site may well share an electron in a similar manner, giving rise to a band-gap surface state. For two electrons trapped at the defect, the ground-state configuration may be characterized by $2Ti^{3+}\cdot V_{Os}$, the paramagnetic first ionization stage by $2Ti^{3+}\cdot V_{Os}{}^{+}$. For simplification, we will denote the defect by $V_{Os}{}^{(+)}$ and corresponding bulk defects by $V_O{}^{(+)}$.

2. Interaction of intrinsic defects with oxygen

The concentration of defects $V_{Os}{}^{(+)}$ also determines characteristic $\Delta\sigma$ and $\Delta\varphi$ changes during O_2 interaction at temperatures below and above the TDS maximum ($T_{max}=400$ K) of chemisorbed oxygen shown in Fig. 3. The following evaluation of $\Delta\sigma$ and $\Delta\varphi$ results makes it possible to separate charge-transfer reactions during formation of $O_2{}^{(-)}$ from charge-transfer reactions during annealing of defects with oxygen atoms that are formed after dissociation of chemisorbed oxygen. This annealing involves both surface and subsurface (bulk) vacancies, according to the relation

$$V_{O(s)}{}^{\delta+}+\delta e+O\rightarrow O_1\ . \tag{19}$$

Here O_1 denotes lattice oxygen of ideal TiO_2. We will start with experimentally observed $\Delta\varphi$ values to calculate concentrations of chemisorbed $O_2{}^-$ from the band bending by assuming $\mu^{ad}(O_2{}^-)=0$ and $\delta(O_2{}^-)=-1$ independent of the coverage. The influence of bulk Fermi-level shifts on shifts in the surface potential for the range of bulk defect concentrations observed in our studies is estimated to be below 10 meV and can thus be neglected even if defect reactions [Eq. (19)] occur simultaneously with chemisorption. From $\Delta\sigma$ we calculate ΔN, which is partly due to band-bending (chemisorption) effects as expected from $\Delta\varphi$ and partly due to defect reactions as characterized in Eq. (19). Comparison of $\Delta\varphi$ and $\Delta\sigma$ values thus makes possible the separation of chemisorption effects, i.e., formation of $O_2{}^-$, from surface and bulk reaction effects, i.e., annealing of oxygen vacancies $V_{Os}{}^{(+)}$ due to dissociative reactions with $O_2{}^-$. From $\Delta\varphi$ and $\Delta\sigma=f(t)$, with typical examples shown in Fig. 3, we determine characteristic increases in the concentration Θ(surf) of chemisorbed $O_2{}^-$ and corresponding decreases in the concentration Θ(vol) of ionized intrinsic defects, most of which are located in subsurface regions.

Typical results are shown in Fig. 10 for $T=303$ and 348 K. Evidently at lower temperatures, chemisorption of O_2 determines the predominant charge-transfer contribution, whereas at elevated temperatures above the maximum of thermal desorption, defect reactions in subsurface regions dominate the total charge transfer. Above 348 K, chemisorption and, hence, trapped surface charges as monitored by $\Delta\varphi$ become extremely small (cf., e.g., $\Delta\sigma$ and $\Delta\varphi$ effects in Fig. 3) and annealing of subsurface defects is the predominant charge-transfer reaction between O_2 and TiO_2(110), which involves free electrons.[2]

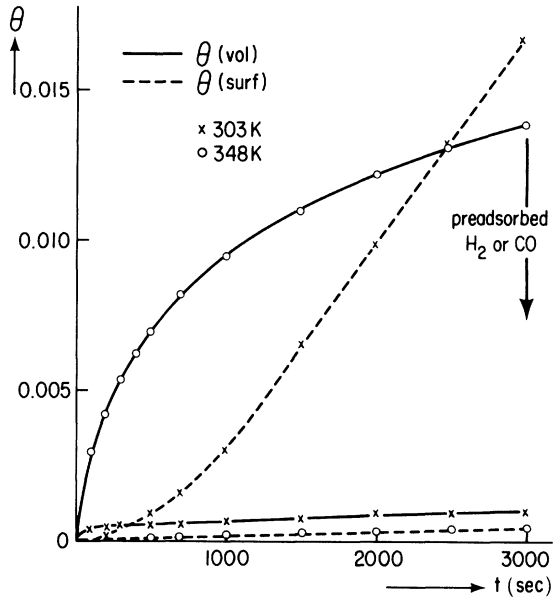

FIG. 10. Changes in the coverage Θ of ionized species, formally determined from changes in the conductivity and work function during oxygen exposure to separate volume Θ(vol) and surface Θ(surf) contributions. [$P(O_2)=6.7\times10^{-4}$ Pa]. Further explanations are given in the text.

3. Interaction of intrinsic defects with other gases

We observed that preadsorbed hydrogen and carbon monoxide reduces Θ(vol) significantly in subsequent oxygen-exposure experiments, whereas Θ(surf) remains unaffected even for an order-of-magnitude reduction of Θ(vol). Evidently reactions between chemisorbed oxygen and oxygen vacancies in subsurface regions are kinetically hindered in the presence of H_2 and CO. Since, in addition, chemisorption of H_2 and CO is possible only in the presence of defects (see Sec. III C), we conclude that intrinsic surface defects act as active sites for chemisorption of H_2, CO, and O_2. In the latter case, annealing processes described by Eq. (19) are involved.

4. Geometry of defects and adsorption complexes

The results of the discussion combined with experimental results from Sec. III B and III C lead us to a suggestion of geometric models for the various adsorption complexes investigated in our study as shown schematically in Fig. 11.

(a) Oxygen vacancies $V_{Os}{}^{(+)}$ are associated with two Ti surface atoms to form $2Ti^{3+}\cdot V_{Os}{}^{+}$ in the first ionization stage. This intrinsic defect is formed by high-temperature treatment or by low-temperature CO exposure to a defect surface at which CO_2 formation occurs by reactions with an adjacent lattice oxygen at an extremely low rate at 300 K and a slightly increasing rate with increasing tem-

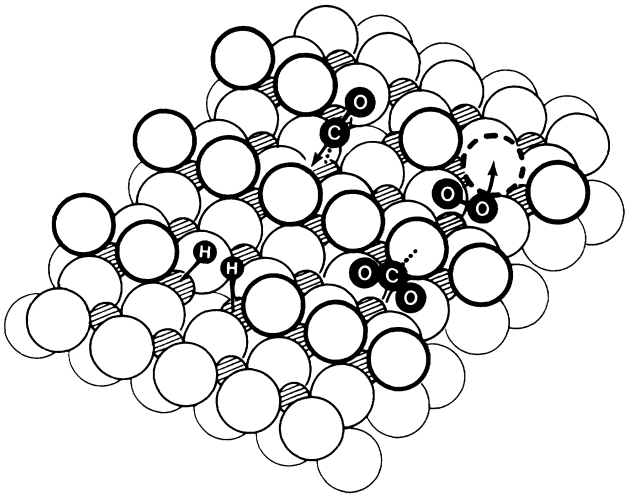

FIG. 11. Geometric model of adsorption complexes and intrinsic defects at TiO_2(110) investigated in this study.

perature, as can be deduced from $\Delta\sigma$ effects in Fig. 4.

(b) During CO exposure at low temperatures, additional oxygen vacancies due to CO_2 formation can be formed only in the vicinity of an already existing oxygen vacancy. As the result of repulsion between the remaining adjacent oxygen vacancies after this surface reaction, one of these point defects diffuses into subsurface layers. This explains the experimentally observed increase in $\Delta\sigma$ with increasing temperature at constant $\Delta\varphi$ (cf. Fig. 4), with the latter given by a constant number of oxygen vacancies as "active" (chemisorption) sites for coadsorption. The CO_2 formed during this interaction desorbs into the gas phase.

(c) The equilibrium position of chemisorbed O_2^- is determined by maximum Coulomb interaction between O_2^- and the ionic lattice. In the presence of positively charged surface donors, i.e., oxygen vacancies, the equilibrium position is indicated in Fig. 11. In this position, dissociation of chemisorbed oxygen is possible even at low temperatures and thereby leads to annealing of surface defects. Above the maximum temperature of thermal desorption, oxygen reacts directly from the gas phase to anneal oxygen vacancies at the surface. Diffusion in the electrochemical potential gradient leads to rapid annealing of vacancies also in subsurface regions.

(d) Chemisorbed hydrogen forms ionic titanium—hydride bonds Ti^{4+}—H^- after dissociation at surface-defect sites. This involves two electrons, which before adsorption were attributed to the intrinsic defect. This type of bond was also deduced from earlier ESD studies.[9] The first ionization stage leads to Ti^{4+}—H bonds. For simplification in this study we have denoted the ground state by H and the first ionization state by H^+ (cf., e.g., Fig. 9).

In subsequent thermal desorption experiments, two hydrogen atoms can easily recombine. This explains the experimentally observed first-order thermal desorption of molecular H_2 after adsorption at low temperatures. The $\Delta\sigma$ effects (cf. Fig. 4) are explained by diffusion of hydrogen atoms into the bulk, thereby forming donor-type defects, i.e., bulk OH— bonds with hydrogen atoms bridging two oxygen atoms.[20] The diffusion occurs after formation of atomic hydrogen adsorption complexes associated with oxygen vacancies. Bulk diffusion leads to an increase in the formally determined partial charge δ with increasing temperature. Bulk reactions with molecular hydrogen, which have been studied systematically[16] at $T > 600$ K, are below the detection limit of even our sensitive $\Delta\sigma$ measurements at 300 K in the absence of oxygen vacancies at the surface. The activation energy to dissociate H_2 is too high in this case and the surface reaction becomes rate limiting.

(e) CO_2 is chemisorbed in an equilibrium position, which does not kinetically hinder the reactions between chemisorbed O_2 and vacancies. In addition, chemisorption equilibria of CO_2 are not influenced by vacancies.

The experimental results presented in this paper suggest the geometric models as shown in Fig. 11. In subsequent photoemission and high-resolution ELS measurements, we will determine electronic and dynamic properties of these complexes to support or modify these simple structure models.

C. TiO_2(110) as a prototype surface to study solid-gas interactions

In our earlier studies we pointed out that ZnO($10\bar{1}0$) serves as an excellent prototype surface to study reversible metal oxide-gas interactions with negligible influence from bulk defects.[11] The present study shows that TiO_2(110) may serve as a prototype surface to study metal oxide-gas interactions including changes in the concentrations of intrinsic as well as extrinsic bulk defects. Characteristic similarities and differences for both surfaces are summarized in Table II and Figs. 12 and 13. Physisorption has been studied so far at ZnO($10\bar{1}0$) only.

Chemisorption leads to characteristic charge-transfer reactions and to the formation of adsorbate complexes at defect-free surfaces. With the exception of CO, all the gases listed in Table II can be desorbed from both ZnO($10\bar{1}0$) and TiO_2(110) surfaces without formation of intrinsic defects. Intrinsic defects, i.e., oxygen vacancies, act as active sites for chemisorption of H_2, O_2, and CO. These active sites make possible the dissociation of H_2 and O_2 even at or below room temperatures.

With the use of high-temperature pretreatment in oxygen, a basically defect-free subsurface region can be produced in ZnO($10\bar{1}0$). Since, in addition, bulk diffusion coefficients are extremely low, subsequent adsorption studies can be done without measureable influence from bulk defects. Incorporation of lattice oxygen to form interstitial oxygen or of hydrogen is energetically unfavorable in ZnO (dashed lines in Figs. 12 and 13). It is also unfavorable for the interaction of stoichiometric defect-free TiO_2 with O_2 (solid line in Fig. 12). It is, however, energetically favorable for the incorporation of hydrogen into the TiO_2 lattice (solid line in Fig. 13). In this case, oxygen vacancies at the surface act as active sites for bulk reactions from the gas phase with significantly reduced activation barriers at the surface (compare thick lines for the defect-free and thin lines in Fig. 13 for the defect surface interacting with H_2). At ZnO surfaces, oxygen va-

TABLE II. Solid-gas interactions for the prototype surfaces $TiO_2(110)$ and $ZnO(10\bar{1}0)$. For simplification, electronic charge-transfer reactions during chemisorption and bulk diffusion are not characterized.

	$TiO_2(110)$	$ZnO(10\bar{1}0)$	
Physisorption $95 \leq T \leq 240$ K		H_2, O_2, CO, CO_2[a]	Reaction (1) in Figs. 12,13
Chemisorption at defect-free surfaces $T=300$ K	$H^{(+)}, O_2^{(-)}$, [CO],[b] CO_2	$H^{(+)}, O_2^{(-)}$, [CO],[b] CO_2[c] $\rightarrow CO_2$[e]	Reaction (2) in Figs. 12,13
Chemisorption at surface defects (oxygen vacancies V_{Os}), $T=300$ K	$H_2 \rightarrow 2TiH^{(+)}$ $O_2 \rightarrow 2O_1 - 2V_{Os}^{(+)}$ $CO \rightarrow CO \cdot V_O^{(+)}$	$H_2 \rightarrow 2ZnH^{(+)}$ $O_2 \rightarrow 2O_1 - 2V_{Os}^{(+)}$ $CO \rightarrow CO \cdot V_O^{(+)}$[d]	Reaction (3) in Fig. 13 Reaction (3) in Fig. 12
Bulk diffusion from surface defect sites $T=300$ K[e]	$[TiH^{(+)}]_{surf} \rightarrow [O-H-O^{(+)}]_{bulk}$ $O_{1,s} \rightarrow O_1 - V_O^{(+)}$		Reaction (4) in Fig. 13 Reaction (4) in Fig. 12
Ratio surface-bulk defects under thermodynamic equilibrium[f] (900 K, $P(O_2)=10^{-4}$ Pa)	1	1000[g]	

[a]Reference 30.
[b]Chemisorbed CO reacts in part with lattice oxygen to form CO_2
[c]References 11, 13, 29, and 30.
[d]References 13, 29, and 31.
[e]Measurements after high-temperature pretreatment in oxygen ($T=1000$ K, $P(O_2)=10^{-4}$ Pa, 500 sec.
[f]Numbers of defects per unit area in the first layer and an arbitrary bulk layer are compared.
[g]References 13 and 36.

cancies act as specific adsorption sites for hydrogen, but the bulk reaction is energetically unfavorable (dashed line and thin solid line for larger z in Fig. 13). The same difference is found for the interaction of oxygen with surface defects shown in Fig. 12. For ZnO, experimental conditions can be chosen to also have bulk reactions at low temperatures. This can be done by high-temperature–low-oxygen-pressure pretreatment and subsequent low-temperature quenching of so prepared subsurface defects under UHV conditions.

The schematic Figs. 12 and 13 contain rough estimates on potential energies. For thermodynamic considerations of, e.g., the temperature dependence of the different solid-gas interactions, the entropy changes have to be considered, too. Entropies increase during formation of defects, they decrease during formation of adsorption complexes, and the compromise between changes in energy and entropy then determines the concentration of particles or defects for the various interaction steps as a function of temperature, partial pressure, and time.

V. CONCLUSIONS

We have investigated the interaction of $TiO_2(110)$ with O_2, H_2, CO, and CO_2. We found that a simple charge-transfer model can be used to formally describe the changes in the free-electron concentration during solid-gas interaction by means of partial charges and dipole moments involved in the formation of adsorbate complexes.

Small deviations from the ideal surface-atom composition due to oxygen vacancies at the surface significantly influence the electronic charge transfer during H_2, CO, and O_2 exposure. Rapid bulk diffusion of hydrogen atoms and oxygen vacancies even at room temperature, and the fact that surface oxygen vacancies act as chemisorption sites for H_2 and CO, have led to modifications of this simple charge-transfer chemisorption model.

We have shown that $ZnO(10\bar{1}0)$ and $TiO_2(110)$ may serve as two prototype surfaces to study metal-oxide–gas interactions. The $TiO_2(110)$ surface may be considered as a prototype surface for rapid gas-bulk reactions in contrast to $ZnO(10\bar{1}0)$ as a prototype surface for negligible gas-bulk reactions at low temperatures.

Characteristic differences between ZnO-gas interactions and the more complex TiO_2-gas interactions result from energetically more favorable bulk reactions and smaller activation barriers for bulk diffusion in TiO_2. The latter takes place in a strong electrochemical potential gradient near the surface. As a result, high concentrations of surface charges and intrinsic defects cannot be accumulated

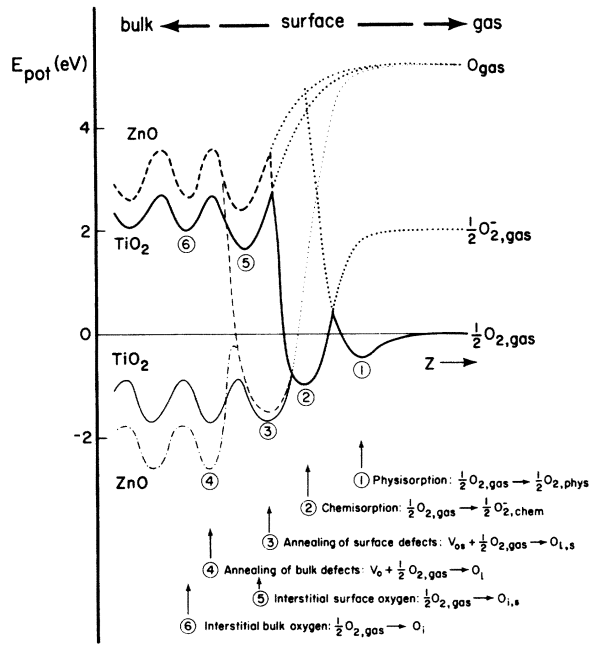

FIG. 12. Characteristic solid-gas interaction steps pictured by the dependence of the potential energy on distance from the surface with several relative minima. The examples characterize O_2 interaction steps with the prototype surfaces TiO_2(110) and ZnO(10$\bar{1}$0), respectively. For simplification, changes in the effective ionization of partly filled donor or acceptor states and corresponding changes in the number of free electrons have not been included in the brief characterization of different reaction steps. These changes are, however, taken into account in Fig. 9 by assuming flat-band conditions ($V_s=0$) during the reaction. For further details, see text.

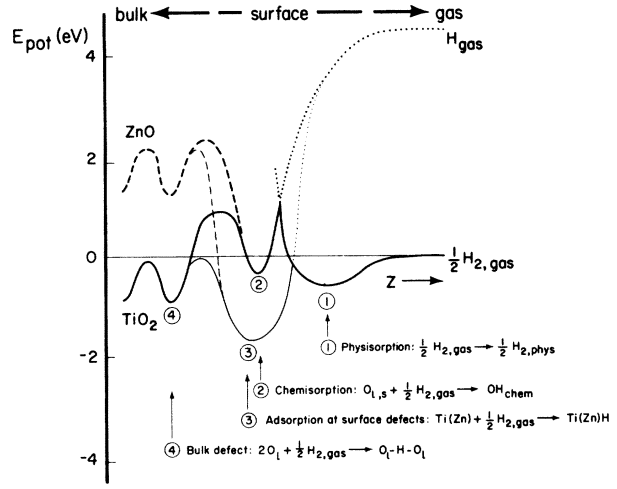

FIG. 13. Same as Fig. 12 for characteristic solid-gas interaction steps between H_2 and TiO_2(110) as well as ZnO(10$\bar{1}$0), respectively. For further details, see text.

at TiO_2(110) surfaces without subsequent bulk reactions occurring, which thus dissipate these charges and defects. Therefore, the electrochemical potential at the surface of TiO_2(110) is basically determined by subsurface, i.e., bulk properties. We believe that this is the atomistic explanation for the surprising reproducibility of TiO_2 semiconductor electrodes.

ACKNOWLEDGMENTS

The assistance of P. Esser and K. Majoni during molecular-flow experiments as well as data evaluation and of J. Schaefer during XPS and EELS studies is gratefully acknowledged. We thank C. Robinson for carefully reading the manuscript. The work was supported by the Deutsche Forschungsgemeinschaft, Fonds der Chemischen Industrie, and a Montana State University grant supported under National Science Foundation Grant No. ISP-80-11449. The LEED, TDS, EPR, and part of $\Delta\sigma$ and $\Delta\varphi$ studies were done at the Institute of Physical Chemistry, University of Hannover, Federal Republic of Germany. The XPS and EELS studies were done at CRISS (Center for Research in Surface Science and Submicron Analysis at Montana State University, Bozeman, Montana) and supported by the National Science Foundation under Contract No. CHE-79-16134.

[1]See, e.g., A. Jujishima and K. Honda, Nature (London) 238, 37 (1972); V. E. Henrich, Prog. Surf. Sci. 9, 143 (1979); *Basic Research Opportunities for Lasting Fuel Gas Supplies, Report from Workshop at Texas A&M University, July, 1981,* edited by C. A. Rodenberger *et al.* (Gas Research Institute, Chicago, 1982); *Solar Energy Conversion: Solid State Physics Aspects,* in Vol. 31 of *Topics in Applied Physics,* edited by B. O. Seraphim, (Springer, Berlin, 1981), and references given there.

[2]H. W. Gundlach and K. E. Heusler, Z. Phys. Chem. N. F., 119, 213 (1980).

[3]R. V. Kasowski and R. H. Tait, Phys. Rev. B 20, 5168 (1979).

[4]V. E. Henrich and R. L. Kurtz, Phys. Rev. B 23, 6280 (1981).

[5]S. Munnix and M. Schmeits, Phys. Rev. B (in press).

[6]V. E. Henrich, G. Dresselhaus, and H. J. Zeiger, Phys. Rev. Lett. 36, 1335 (1976); Solid State Commun. 24, 623 (1977).

[7]V. E. Henrich, G. Dresselhaus, and H. J. Zeiger, J. Vac. Sci. Technol. 15, 534 (1978).

[8]J. B. Goodenough, Metallic Oxides, in *Progress in Solid State Chemistry,* edited by H. Reiss (Pergamon, New York, 1972).

[9]M. L. Knotek, Surf. Sci. 91, L17 (1980); 101, 334 (1980).

[10]W. J. Lo, Y. W. Chung, and G. A. Somorjai, Surf. Sci. 71, 199 (1978).
[11]W. Göpel, *Advances in Solid State Physics XX* (Vieweg, Braunschweig, 1980) p. 177.
[12]W. Göpel and G. Rocker, J. Vac. Sci. Technol. 21, 389 (1982).
[13]W. Göpel and U. Lampe, Phys. Rev. B 22, 6447 (1980).
[14]R. Haul and G. Dümbgen, J. Phys. Chem. Solids 26, 1 (1965).
[15]M. L. Knotek, in *Proceedings of the Symposium on Electrode Materials and Processes for Energy Conversion and Storage,* edited by F. D. E. McIntyre, S. Srinivesen, and G. Will (The Electrochemical Society, Princeton, New Jersey, 1977), Proc. Vol. 77-6.
[16]O. W. Johnson, S. H. Paek, and J. W. DeFord, J. Appl. Phys. 46, 1026 (1975).
[17]F. A. Kröger, *The Chemistry of Imperfect Crystals* (North-Holland, Amsterdam, 1964).
[18]G. A. Acket and J. Volger, Physica (Utrecht) 29, 225 (1963); 30, 1667 (1964); 32, 1680 (1966).
[19]V. N. Bogomolov, Fiz. Tvrd. Tela (Leningrad) 5, 2011 (1963) [Sov. Phys.—Solid State 5, 1468 (1964)].
[20]A. R. Van Hippel, J. Kalnajs, and W. B. Westphal, J. Phys. Chem. Solids 23, 779 (1962).
[21]H. Yamada and G. R. Miller, J. Solid State Chem. 6, 169 (1973).
[22]R. D. Shannon, J. Appl. Phys. 35, 3414 (1964).
[23]G. B. Acket and J. Volger, Phys. Lett. 8, 244 (1964).
[24]D. C. Cronemeyer, Phys. Rev. 87, 876 (1952).
[25]W. Jakubowski, Acta Phys. Pol. 33, 465 (1968).
[26]S. Andersson, B. Collen, U. Kuylenstierna, and A. Magneli, Acta. Chem. Scand. 11, 1641 (1957).
[27]P. G. Wahlbeck and P. W. Gilles, J. Am. Ceram. Soc. 49, 188 (1966).
[28]L. J. Van der Pauw, Philips Res. Rep. 13, 1 (1958); Philips Tech. Rev. 20, 220 (1958).
[29]See, e.g., W. Hotan, W. Göpel, and R. Haul, Surf. Sci. 83, 162 (1979) and references given there.
[30]P. Esser and W. Göpel, Surf. Sci. 97, 309 (1980).
[31]F. Runge and W. Göpel, Z. Phys. Chem. N. F. 123, 173 (1980).
[32]W. Göpel, J. A. Schaefer, and G. Rocker, Surf. Sci. (in press).
[33]N. P. Bogoroditskii, V. Kristya, and Ya. I. Panova, Fiz. Tverd. Tela (Leningrad) 14, 302 (1966) [Sov. Phys.—Solid State 9, 187 (1967)]; A. K. Ivukina and Ya. I. Panova, *ibid.* 10, 622 (1966) [6 311 (1967)]; J. H. Becker and W. R. Hosler, Phys. Rev. 137, A1872 (1965); G. B. Acket and J. Volger, Phys. Lett. 8, 244 (1964); R. G. Breckenridge and W. R. Hosler, Phys. Rev. 91, 793 (1953); J. H. Becker and W. R. Hosler, J. Phys. Soc. Jpn. Suppl. 18, 152 (1963); E. H. Greener *et al.*, J. Am. Ceram. Soc. 48, 623 (1965); R. N. Blumenthal *et al.*, J. Phys. Chem. Solids 27, 643 (1966); L. A. K. Dominik and R. K. MacCrone, Phys. Rev. 156, 910 (1967); W. R. Thurber and J. H. Mante, Phys. Rev. 139, A1655 (1965); G. A. Acket and J. Volger, Physica (Utrecht) 32, 1680 (1966); M. Itakura *et al.*, Jpn. J. Appl. Phys. 6, 311 (1967); G. A. Acket and J. Volger, Physica (Utrecht) 30, 1667 (1964); I. Bransky and D. S. Tannhauser, Solid State Commun. 7, 245 (1969); M. I. Klinger, Phys. Status Solidi 27, 479 (1968); V. N. Bogomolov and V. P. Zhuze, Fiz. Tverd. Tela (Lennigrad) 12, 444 (1966) [Sov. Phys.—Solid State 8, 1904 (1967)]; T. Goto and T. Okada, J. Phys. Soc. Jpn. 25, 289 (1968); V. N. Bogomolov *et al.*, Fiz. Tverd. Tela (Leningrad) 9, 3175 (1967); J. Yahia, Phys. Lett. 23, 425 (1966); Z. M. Jarzebski, *Oxide Semiconductors,* (Pergamon, New York, 1973); M. G. Harwood, B. J. Appl. Phys. 16, 1493 (1965); J. A. van Raalte, J. Appl. Phys. 36, 3365 (1965); H. B. Whitehurst *et al.*, J. Phys. Chem. Solids 28, 861 (1967); V. N. Bogomolov and V. P. Zhuse, Fiz. Tverd. Tela (Leningrad) 8, 2390 (1966); F. A. Kröger, *The Chemistry of Imperfect Crystals* (North-Holland, Amsterdam, 1964).
[34]V. N. Bogomolov and V. P. Zhuse, Fiz. Tverd. Tela. (Leningrad) 10, 100 (1962) [Sov. Phys.—Solid State 5, 2404 (1963).]
[35]H. P. R. Frederikse, J. Appl. Phys. Suppl. 32, 2211 (1961).
[36]W. Göpel, J. Vac. Sci. Technol. 15, 1298 (1978).
[37]W. Göpel, J. Vac. Sci. Technol. 16, 1229 (1979).